

A One-Step Biofunctionalization Strategy of Electrospun Scaffolds Enables Spatially Selective Presentation of Biological Cues

Paul Wieringa, Andre Girao, Maqsood Ahmed, Roman Truckenmüller, Alexander Welle, Silvestro Micera, Richard van Wezel, and Lorenzo Moroni*

To recapitulate the heterogeneous complexity of tissues in the human body with synthetic mimics of the extracellular matrix (ECM), it is important to develop methods that can easily allow the selective functionalization of defined spatial domains. Here, a facile method is introduced to functionalize microfibrillar meshes with different reactive groups able to bind biological moieties in a one-step reaction. The resulting scaffolds prove to selectively support a differential neurite growth after being seeded with dorsal root ganglia. Considering the general principles behind the method developed, this is a promising strategy to realize enhanced biomimicry of native ECM for different regenerative medicine applications.

extracellular matrix (ECM), many traditional biofabrication strategies also do not capture the nuanced heterogeneous complexity of native cellular environments in a controlled manner. This limits the possibility of inducing relevant cell responses, preventing the adequate study of more complex biological systems and posing a barrier to further tissue scaffold development. In response, 3D culturing environments have been developed that exhibit controlled patterns of biologically relevant cues, including the immobilization of cell adhesion molecules in heterogeneous 3D patterns^[2] and the formation of complex 3D structures.^[3,4]

1. Introduction

The intrinsic heterogeneity of the body poses a great challenge when attempting to restore or replace lost functions. An emerging perspective in both biological sciences and tissue scaffold design is the influence of the microenvironment on cellular and tissue function.^[1] While the traditional 2D culturing environment fails to replicate the complex and multifaceted 3D environment of the

Of the various scaffold fabrication strategies available, electrospinning (ESP) is often cited as a promising method of recreating the fibrous structure of the natural extracellular matrix (ECM).^[5] ESP scaffolds have proven to be particularly promising for neural tissue engineering applications.^[6] By changing various parameters, this process can form fibers from tens of nanometers to tens of micrometers and can produce both randomly or oriented patterns of fibers. However, these fibers must

Dr. P. Wieringa, A. Girao, Dr. M. Ahmed, Prof. R. Truckenmüller, Prof. L. Moroni
Department of Tissue Regeneration
MIRA Institute for Biomedical Technology and Technical Medicine
University of Twente
Enschede 7500AE, The Netherlands
E-mail: l.moroni@maastrichtuniversity.nl

Dr. P. Wieringa, Prof. R. van Wezel
Department of Biomedical Signals and Systems
MIRA Institute for Biomedical Technology and Technical Medicine
Twente University
Enschede 7500AE, The Netherlands


Dr. P. Wieringa, Prof. S. Micera
BioRobotics Institute—Scuola Superiore Sant'Anna
Pisa 56127, Italy

P. Wieringa
Istituto Italiano di Tecnologia
Center for Micro-BioRobotics @SSSA
Viale Rinaldo Piaggio 34, Pontedera, Pisa 56025, Italy
Prof. R. Truckenmüller, Prof. L. Moroni
Department of Complex Tissue Regeneration
MERLN Institute for Technology-Inspired Regenerative Medicine
Maastricht University
Maastricht 6200 MD, The Netherlands

Dr. A. Welle
Institute of Functional Interfaces (IFG)
and Karlsruhe Nano Micro Facility (KNMF)
Karlsruhe Institute of Technology (KIT)
Eggenstein-Leopoldshafen, Karlsruhe 76344, Germany

Prof. S. Micera
Translational Neural Engineering Laboratory
Center for Neuroprosthetics and Institute of Bioengineering
School of Engineering
Ecole Polytechnique Federale de Lausanne
Lausanne 1015, Switzerland

Prof. R. van Wezel
Biophysics
Donders Institute for Brain
Cognition and Behaviour
Radboud University
Nijmegen 6525 AJ, The Netherlands

 The ORCID identification number(s) for the author(s) of this article can be found under <https://doi.org/10.1002/admt.202000269>.

© 2020 The Authors. Published by Wiley-VCH GmbH. This is an open access article under the terms of the Creative Commons Attribution-NonCommercial License, which permits use, distribution and reproduction in any medium, provided the original work is properly cited and is not used for commercial purposes.

DOI: 10.1002/admt.202000269

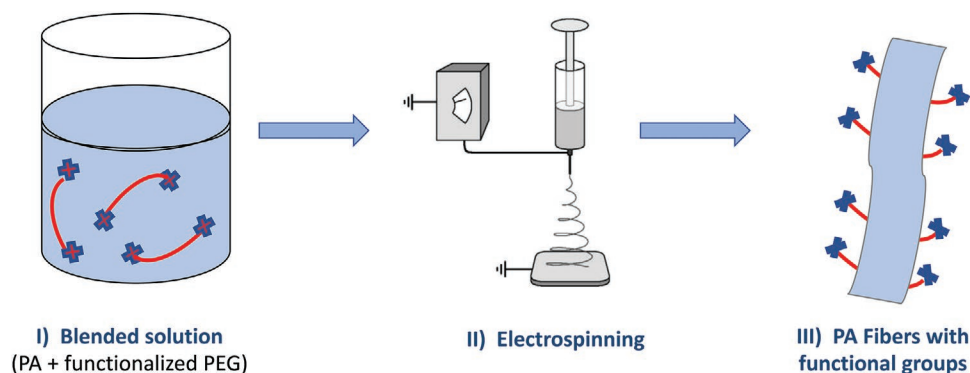


Figure 1. Preparation of the functionalized ESP fibers. I) The blended ESP polymer solution is first prepared, with the addition of short polymer chains (red), homofunctionalized with reactive species (blue crosses), to the bulk polymer solution. II) This solution is then used in the electrospinning process, where III) the resulting fibers exhibit reactive groups on the fiber surface.

often be modified to present cell adhesion moieties or other cues in order to better approximate the native ECM.^[7] These are typically affixed to the fiber surface by the physical adsorption of proteins, chemical conjugation of biomolecules, or by incorporating ECM proteins, such as collagen, into the polymer solution. While physical adsorption is relatively unstable, a blended fiber can require a large amount of protein mixed into the organic solvent of the polymer solution. This mixing potentially denatures the protein and renders it nonfunctional; as a result, this approach is expensive and potentially ineffective. The bioconjugation approach typically requires the surface of ESP fibers to be modified with reactive groups; fibers are then exposed to a solution of biomolecules, which chemically bind to the reactive groups they encounter. This method remains an efficient and effective means of fiber functionalization. However, this approach homogeneously functionalizes the entire scaffold structure and cannot be used to impart a spatially defined pattern onto the fibrous construct.

Spatially selective patterns can also be achieved by photolithographic means, though this can lead to inefficient conjugation and polymer degradation.^[8–11] Furthermore, conjugation only occurs on surfaces that are efficiently exposed to radiation, limiting this application to only the superficial “visible” regions of 3D fibrous scaffolds. Here, we present an approach to create “prefunctionalized” ESP fibers, whereby poly(ethylene glycol) (PEG) chains homofunctionalized with reactive groups are introduced to the polymer solution of a chosen biomaterial a priori the ESP process (Figure 1). Three different reactive groups are characterized: i) nonselective succinimidyl valerate (SVA, an *N*-hydroxysuccinimide variant) for amine conjugation, ii) a more selective thiol-maleimide conjugation approach, and iii) a bio-orthogonal alkyne-azide “click chemistry” strategy. The use of small chain PEG as a carrier results in the presentation of functional groups on the fiber surface without additional processing required, representing a simple method for achieving functionalized fibers.

When the different fibers are fabricated into a single construct, this provides a powerful method to selectively functionalize specific subsets of fibers within a scaffold. Combined with patterned ESP techniques, this creates a spatially defined arrangement of functionalized fibers that ensures the entire fiber surface is activated. We verified the ability to create spatially defined functionalization within a fibrous architecture and examine neurite growth on scaffolds functionalized with

the peptide sequence H-Gly-Arg-Gly-Asp-Ser-OH (RGD) or the laminin-derived sequence H-Arg-Asn-Ile-Ala-Glu-Ile-Ile-Lys-Asp-Ile-OH (RNIAEIIKDI, P20).^[12] Homogeneously functionalized scaffolds successfully supported neurite growth, with no statistical difference in growth observed between peptides. However, a scaffold functionalized with both peptides in a spatially defined manner was shown to produce spatially modulated neurite growth, underscoring the value of employing complex ECM-mimicking environments to further elucidate cell behavior.

2. Results

Initial ESP trials incorporated functionalized PEG additives at a concentration of 5% w/v. However, the quality of the fiber deposition across the gap electrode was inconsistent. An apparent phase separation of the blended polymer solution was also observed over time and noted to be dependent on the presence of functional groups, suggesting poor solubility of functional PEG additives at this concentration 5%w/v (see Figures S2 and S3, Supporting Information).

Reducing the additive concentration to 2% produced a stable polymer solution (Figure S4, Supporting Information) and an improved ESP fiber deposition (Figure 2). ALK and SH fibers produced fibers of 0.88 ± 0.23 and 0.71 ± 0.19 μm in diameter, with a statistically significant difference between the two populations. The SVA fibers were much larger in comparison, with a diameter of 1.56 ± 0.47 μm . Image analysis of fiber alignments provides a coherence metric between 0 (random) and 1 (aligned). ALK and SH fibers were found to have statistically similar degrees of alignment (0.42 ± 0.06 and 0.35 ± 0.07 , respectively), while the SVA fibers exhibited a higher degree of alignment (0.59 ± 0.08).

ToF-SIMS analysis provides a method to identify elemental composition of the first few nanometer of a surface, providing an effective means of assessing functional group availability on the pre-functionalized ESP fibers. Plain PA fibers were characterized by several molecular fragments based on the EO repeating units. Moreover, a rather large fragment of the PEOT block, assigned to $[(\text{C}_2\text{H}_4\text{O})_7 \text{C}_7\text{H}_5\text{O}_2]^-$, was detectable in negative polarity SIMS. Based on the matching ^{13}C isotope pattern in the mass spectrum the multiplet would correspond to the most abundant PEOT block after cleavage of the terminal CO group

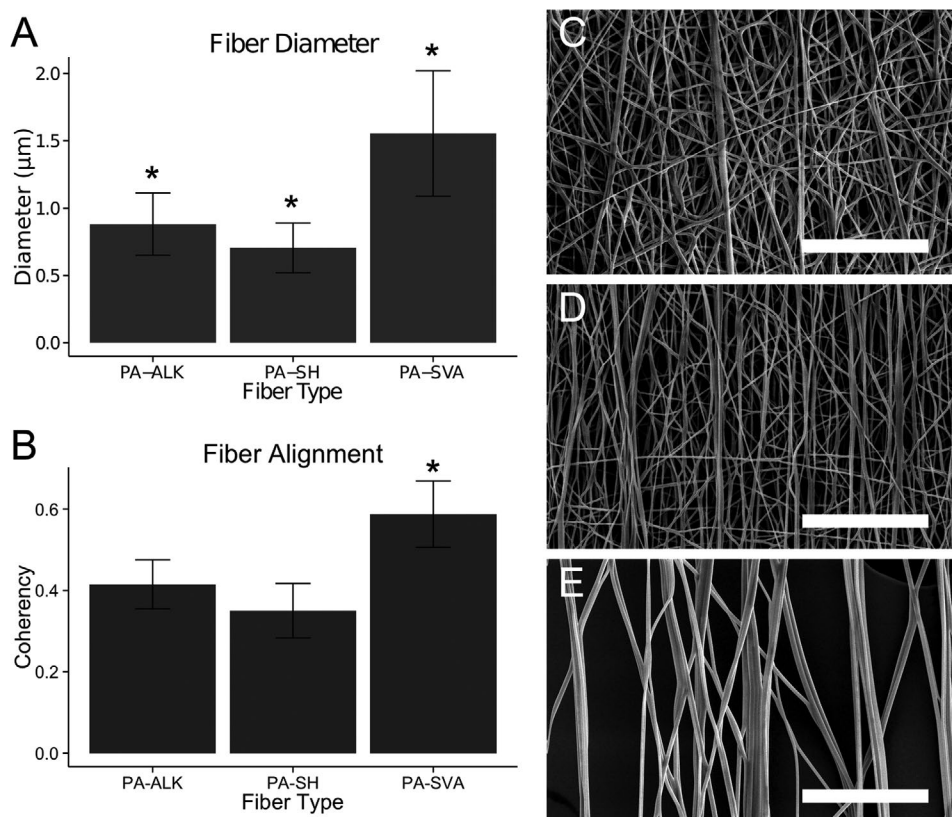


Figure 2. ESP fiber size and alignment. A) Diameters are shown for PA fibers with 2% of ALK, SH, and SVA conjugation agents. All three diameters were found to be statistically different from each other, according to a one-way ANOVA with a posthoc Holm-corrected pairwise comparison ($p < 0.01$; $n = 100$ fibers per sample). B) The degree of fiber alignment was also determined using coherence as a metric, where 0 is random and 1 is perfectly aligned. Fiber alignments of the ALK and SH fibers were found to be similar, while the SVA fibers were significantly more aligned ($p < 0.01$, $n = 6$, 5 images per sample). Example images of C) PA-ALK fibers, D) PA-SH fibers, and E) PA-SVA fibers. Scale bars: 50 μm .

and ionization by hydrogen uptake. Despite their low abundance both the 2% SVA and 2% SH fibers clearly exhibited available functional groups, being absent in plain PA samples. Strong and characteristic signals were, among others, the $\text{C}_4\text{H}_4\text{NO}_2^-$ fragment found for the succinimidyl group of SVA; and S^- together with SH^- in case of the thiol presenting fibers, SH. In secondary ion mass spectra recorded with high mass resolution no interfering signals were present in case of the marker signals given above. Hence, it was possible to record SIMS images with high lateral resolution in a nonbunched mode providing only nominal mass resolution as shown in **Figure 3**. Unfortunately, ALK fibers were not possible to be assessed because the chemical signature of the incorporated alkyne groups was not sufficiently distinct to be discerned from the bulk PA polymer.

To ascertain whether chemical groups on the fiber surface were available for conjugation, solutions of fluorescent probes with complementary conjugation molecules were employed; these included BSA-FITC for SVA conjugation, Dylight-488 with maleimide for SH conjugation and Megastokes 678 with an azide for alkyne (ALK) conjugation. Available groups on the fiber surface were reactive (**Figure 4**). The SVA fibers were shown to strongly retain the BSA-FITC protein (Figure 4A) compared to the ALK and SH fibers (Figure 4D,G), although a degree of nonspecific binding could still be observed. A high degree of selective conjugation was noted for the smaller molecular probes

used for the ALK fibers (Figure 4F), with no observable cross-reactivity with either the SVA fibers (Figure 4C) or SH fibers (Figure 4I). Similarly, the maleimide fluorescent probe showed a clear preference for the SH fibers (Figure 4H) compared to no observed reactivity with the SVA or ALK fibers (Figure 4B,E).

T-ESP was also employed to create a heterogeneous scaffold of two aligned fiber populations positioned next to each other with defined overlapping region (Figure 4J). A T-ESP scaffold of ALK and SH fibers was exposed to a solution of maleimide-Dylight 488 and azido-MegaStokes 673, verifying that spatially selective conjugation of different fibers types is possible with such a system.

To validate these conjugation strategies, neurite outgrowth was evaluated on functionalized scaffolds. The SH and ALK fibers were selected for in vitro evaluation, owing to similarities of fiber diameter and alignment as well as high conjugation selectivity and similar use of activated proteins. SH fibers and ALK fibers were functionalized with the RGD and P20 peptides, respectively.

Neurite outgrowth on these substrates was well aligned in the direction of fiber orientation (**Figure 5A,B**), with relatively large variability between samples and no distinct differences in neurite length for fibers functionalized with either the RGD or P20 peptide (Figure 5C). The migration of Schwann cells from the explanted tissue was also observed on both fiber substrates,

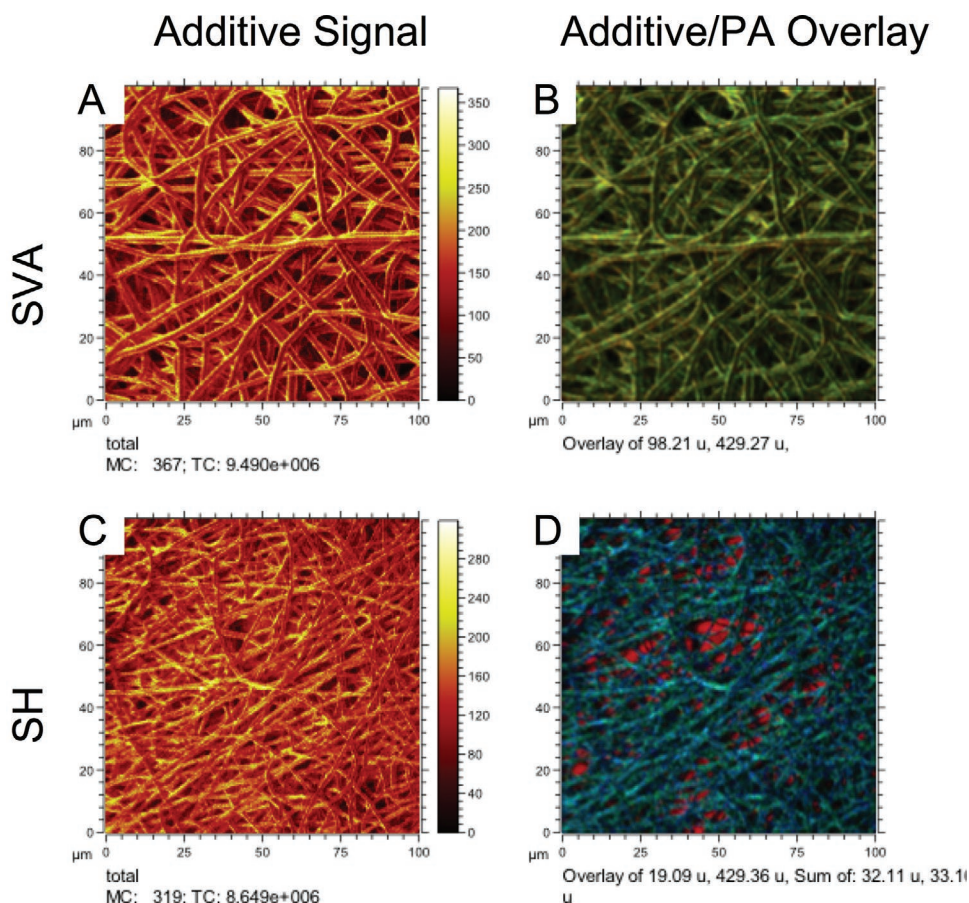


Figure 3. High lateral resolution ToF-SIMS imaging. A,C) Total ion images of SVA and SH fibers, respectively. B) Overlay for SVA sample. Red: succinimidyl moiety $C_4H_4NO_2^-$; green: multiplet at 429 m/z indicating the PEOT block in PA polymer. D) Overlay for SH sample: Red: F^- from the substrate; green: sum of S^- and SH^- ; blue: multiplet at 429 m/z indicating PEOT repeating unit in PA polymer.

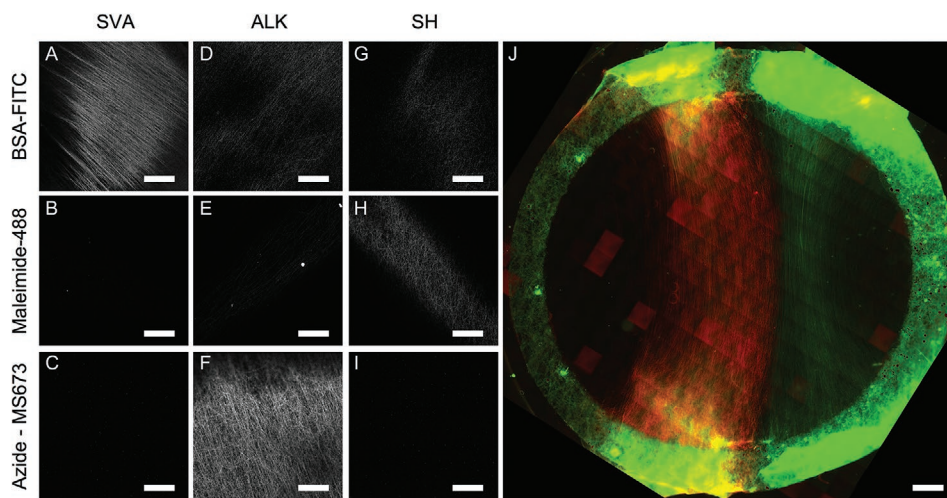


Figure 4. Fluorescent probe conjugation on different fiber types. The SVA additive fibers showed strong binding to A) BSA-FITC, where BSA is a representative large globular protein with available amine groups. No signal was observed when the B) maleimide dye or C) azide dye were applied to SVA fibers. ALK and SH fibers both experienced residual adhesion of D,G) the BSA. The azide-MegaStokes 673 (MS673) and Maleimide-Dylight 488 (Maleimide-488) dyes were shown to have the expected specific affinity to the F) ALK fibers and H) SH fibers, respectively. J) A T-ESP scaffold of ALK and SH fibers within a mesh frame (autofluorescent green boundary) showed selective conjugation of azide-MegaStokes 673 (red) and maleimide-Dylight 488 (green), respectively. Scale bars: A–I) 250 μm ; J) 1 mm.

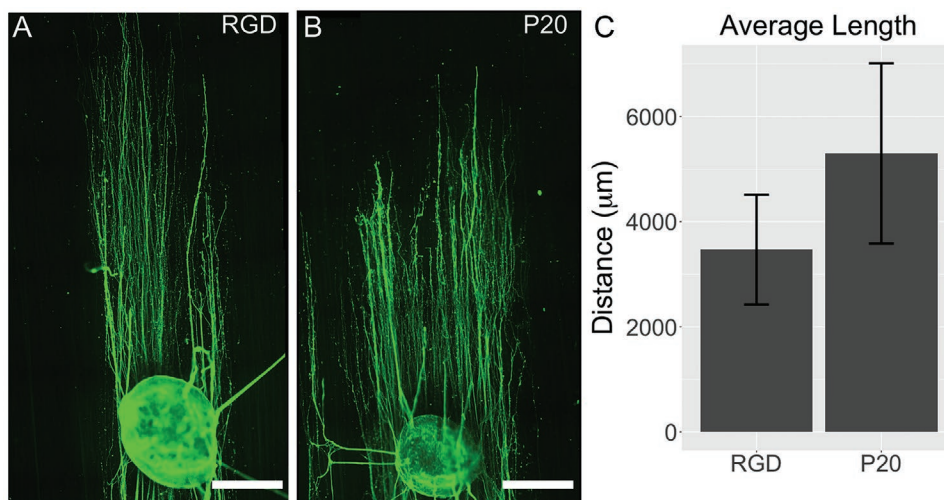


Figure 5. Representative images of neurite outgrowth from explanted DRGs. Neurites outgrowth over a 5 d period on the A) RGD fibers or B) P20 fibers appeared to show a preference for the P20 substrate, C) with average neurite growth of 3469.9 ± 1043.6 and 5298.4 ± 1715.7 μm , respectively. However, further analysis revealed this growth was shown to be statistically equivalent ($n = 3$, Mann–Whitney–Wilcoxon, $p < 0.05$). Scale bars: 500 μm .

with no discernable differences in distance travelled between conditions (Figure S5, Supporting Information).

In contrast, **Figure 6** shows a clear difference in neurite growth when DRGs are presented with both peptides at the same time; divergent T-ESP scaffolds were combined with the one-step functionalization approach to create spatially defined regions of oriented fiber with selective biomolecule activity

(Figure S6, Supporting Information). Under these conditions, a preferential growth on P20-modified fibers was revealed, despite the presence of the cell adhesive RGD peptide. Interestingly, an apparent uniform distribution of migrating Schwann cells was also observed between conditions. To see if the effect was related to intrinsic differences between the ALK- and SH-modified fibers, neurite growth was also compared on divergent

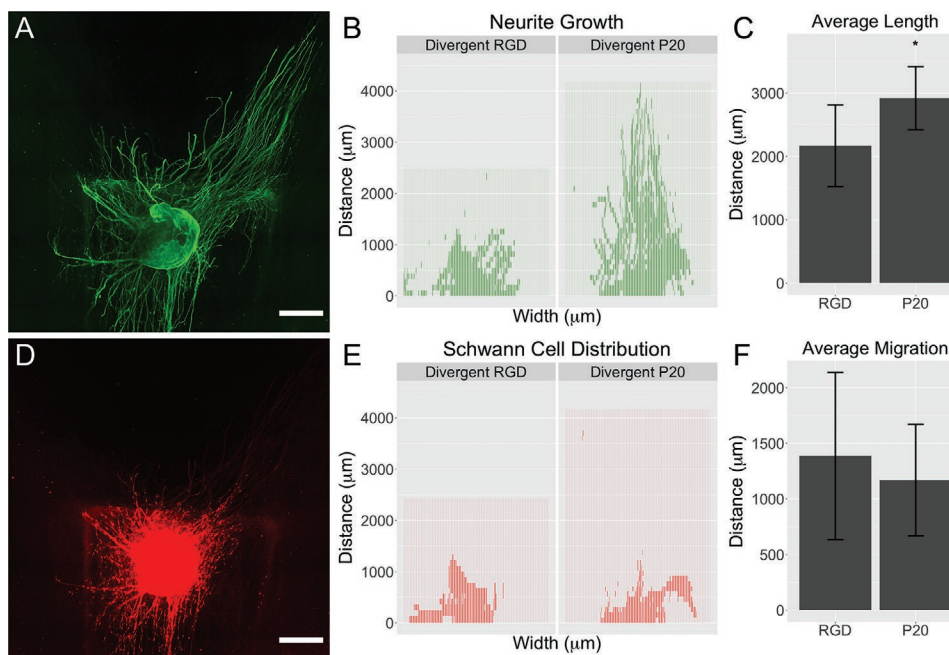


Figure 6. A divergent T-ESP substrate shows preferential neurite growth capitalizing on the one-step functionalization strategy. A) Neurite growth of a 5 d period on heterogeneously functionalization scaffold with a distinct RGD region and a distinct P20 regions, with relative growth (2168.0 ± 643.0 and 2917.6 ± 499.0 μm , respectively) showing a clear preference for growth on the P20-functionalized area. B) A spatial map of growth direction is used C) to quantify aspects of neurite growth (C, $n = 4$, Mann–Whitney–Wilcoxon, $p < 0.05$). Quantified maximum neurite length reveals a consistent and statistically significant preference for P20-functionalized fibers. D) Imaging the same scaffolds for Schwann cell and E) subsequent analysis of distribution revealed no significant differences in Schwann cell migration with average migration distances of 1385.4 ± 749.8 and 1168.9 ± 499.7 μm for RGD and P20, respectively (F, $n = 4$, Mann–Whitney–Wilcoxon, $p < 0.05$). Scale bars: 500 μm .

scaffolds which were not conjugated with any peptide (Figure S7, Supporting Information), however no differences in neurite length were observed when fibers were not functionalized.

3. Discussion

The goal of this study was to develop ESP fibers that could be functionalized with biomolecules without the need of post-modification by wet chemistry or photolithography. While representing a simple strategy for fiber bioconjugation, this was pursued to create fibers with orthogonal conjugation chemistries to enable the selective functionalization of specific subpopulations of fibers within a heterogeneous ESP scaffold. We were able to verify the presence of reactive species on ESP fibers and confirm the selectivity of the different chemistries employed. Applying this approach to the assembly of spatially defined heterogeneous fiber scaffolds, created via the T-ESP technique, a fibrous scaffold with spatially defined, orthogonal conjugation chemistries was created. As an example, preliminary results showed that neurite growth on such scaffolds differed compared to homogeneous scaffold and exhibited spatially modulated behavior.

The ability to conjugate biomolecules to 3D culturing platforms in a spatially defined manner represents a promising tool to study and dictate cell response. While studies of cells on 2D substrates with biomolecule patterns have produced interesting results,^[13,14] planar substrates limit the applicability of these outcomes. Many of the relevant signals imparted to a cell are lost or altered when moving between a native 3D ECM and a 2D substrate. However, the creation of analogous biomolecular patterns within a 3D scaffold via spatial selectivity represents a biofabrication challenge, with emerging strategies employing two-photon activation of reactive molecules within optically-permeable hydrogel environments.^[2,15,16]

Outlined in this current study is a method to impart specific bioactive moieties within a 3D fibrous scaffold, providing cells with a combination of nanotopography and a defined distribution of specific biomolecular cues. Functionalization of ESP fibers traditionally relies on wet chemistry to bestow reactive groups on the fiber surface, a method that does not permit spatially defined bioconjugation. Alternative approaches to functionalize ESP fibers have been explored whereby the polymer solution was modified to include functionalized reactive groups before ESP, either by modifying the polymer directly or by including smaller reactive polymers within the solution. These approaches included conjugation chemistries similar to those employed in the current study.^[17–20] However, all methods required the custom synthesis of reactive polymer chains.

In contrast, the method described in the current study provides a simple means of attaining pre-functionalized ESP fibers through the use of commercially available modified PEG chains as a carrier. Considering the composition of the PA polymer includes segments of PEG, the additional PEG additives are largely miscible with this polymer and allows for entanglement and physical entrapment of the added PEG chains within the bulk of the PA polymer. Despite this bulk incorporation, ToF-SIMS analysis revealed that reactive groups were still available on the fiber surface and their reactivity was confirmed by the

successful conjugation of fluorescent probes; in the case of the ALK group, which could not provide a sufficiently distinct chemical signature for ToF-SIMS detection, selective conjugation of an azide-conjugated dye validated that this group was on the surface and was still reactive.

By using PEG additives with specific functional groups, we show that these functional groups are present on the surface of the resulting fibers. We first showcased the incorporation of PEG-SVA an *N*-Hydroxysuccinimide variant that reacts to the primary amines found in most proteins and peptides, providing a means of nonselective bioconjugation. For a more selective approach, we also validated the incorporation of PEG-SH such that the thiol (–SH) groups are present on the fiber surface and can be reacted with maleimide; by activating a protein or peptide of choice with a commercially available maleimide linker, we achieved selective conjugation to our fiber surface. Similarly, we showed that the incorporation of PEG-ALK provides alkyne groups on the fiber surface which can be reacted with azide-activated species through well reported Alkyne-Azide “click chemistry.” We showed that these approaches are not only biocompatible, but that the reactive groups persist and the PEG additives are not leached out over time; after 5 d in culture medium and 2 d of intense washing during immunohistochemistry preparations, there still remained reactive groups available for conjugation (Figure S6C, Supporting Information).

This approach is compatible with many polymer preparations currently used in ESP and creates fibers nearly identical in composition while varying surface reactivity by simply modifying the used additive. However, the concentration and solubility of the PEG additive must be considered with respect to the polymer/solvent system used. As described here, a high concentration of additive may result in phase separation of the polymer solution prior to the electrospinning process and inconsistent fiber formation. Also observed in this study was an effect of the additive on fiber morphology and alignment, in particular the increased fiber diameter and fiber alignment of the PEG-SVA fibers. As has been widely reported and also previously observed for the T-ESP process, changes to the polymer solution properties often affect the final fiber diameter, including solution viscosity, conductivity, and surface tension.^[21,22] Such changes to the polymer solution through the addition of the SVA additive could account for the increase in fiber diameter. It was also previously observed that molecular entanglement of the bulk polymer, when no solvent is present, correlates with fiber alignment during the T-ESP process.^[21] Similarly, such an additive could conceivably alter polymer chain interaction in the bulk polymer, influencing fiber formation and, thereby, affecting fiber alignment. Thus, while the composition of the fibers maybe seem largely the same, one must take into account the potential effects an additive could have on fiber morphology.

Neurite growth from explanted rat DRGs was evaluated on scaffolds conjugated with either P20 or RGD peptides. Although a possible trend was observed suggesting increased neurite growth on P20 substrates, no statistically significant differences in the degree of outgrowth could be ascertained. To take full advantage of this functionalization approach, a heterogeneous scaffold comprised of two diverging populations of aligned fibers was created such that the effects of each peptide

could be simultaneously evaluated on the same DRG. One fiber type incorporated the ALK additive and was subsequently functionalized with P20 using click chemistry, while the other contained the SH additive and functionalized with the RGD adhesion motifs via thiol-maleimide chemistry. An explanted DRG was then placed on the overlapping region between these two fiber groups, providing neurite outgrowth with a decision point. Similar to the homogeneously conjugated scaffolds, biased neurite growth was observed on the P20-functionalized fiber population, however shown to be statistically significant in this context.

RGD is a well-known cell adhesion peptide sequence, present in many ECM proteins such as fibronectin, vitronectin, collagen, and laminin.^[23] This adhesion molecule is known to interact with cells through a well characterized family of integrins, with clear evidence of positive influence on neurite outgrowth.^[24] In contrast, P20 is a lesser known sequence found specifically on the gamma 1 chain of laminin. Identified by Liesi et al. as promoting neurite outgrowth,^[12] it is now known to bind to the nonintegrin cell membrane prion protein (PrPc). This receptor is considered a modulator of cell behavior, maintaining the destabilization of $\beta 1$ integrin-related point contact (focal adhesion) formation and causing localized release of Ca^{2+} ions, resulting in increased cell motility and neurogenesis.^[25]

The DRG explant model used in this study also includes the complex interaction between neurons and supporting glial Schwann cells, also present in DRG explants and highly active during peripheral nerve regeneration. After injury, Schwann cells typically precede the regenerative front in vivo. They change phenotype to produce ECM molecules and diffusible growth factors, encouraging and guiding neurite growth.^[26] Recent work in our lab has shown that Schwann cells exhibit a response to both the P20 and RGD peptides. While both of these peptides promoted increased metabolic and proliferative activity in comparison to nonfunctionalized fibers, the RGD sequence was observed to also upregulate NGF production.^[27]

Within the current study, the observed bias in neurite growth toward the P20-activated fibers is thought to be the result of the direct effects of P20 on point contact adhesion dynamics and intracellular calcium levels of emerging neurites. While many cues can influence point contact adhesions and, thus, neurite extension,^[28] it has been previously shown that “too stable” adhesion also prevents response to environmental cues and neurite extension.^[29] Thus, despite a localized release of NGF by Schwann cells in response to RGD-conjugated fibers, the effects of P20 dominate and allow neurites achieve more extension. In addition, a recent report has described the paracrine signaling between axons which further promotes neurite extension, indicating that “growth begets growth” and suggesting that an initial bias in growth would continue to persist.^[30]

For scaffolds that are homogeneously functionalized with either RGD or P20, no statistical preference could be found despite initial indications of a preference for P20. However, using tandem-spun scaffolds to create a spatially defined distribution of the different peptides revealed a significant preference for P20 fibers. This is despite virtually no difference in the distribution of Schwann cells in and around the DRG, suggesting that both peptides have equal effect on this glial subtype.^[26] Further examination reveals that neurite growth on

homogeneous scaffolds are altogether longer compared to heterogeneous tandem scaffolds. This could be the result of the tandem “decision point” causing a delay in outgrowth or simply attributed to biological variation between explanted DRGs. This highlights yet another key feature of this selective functionalization strategy: the ability to create more complex microenvironments so the “same” biological sample (e.g., the same DRG) can be simultaneously exposed to multiple cues. This allows one to limit the influence of biological variation and further strengthens the conclusions that can be drawn.

When this approach is implemented within a heterogeneous scaffold, it presents a promising approach to design and investigate complex heterogeneous growth environments. The findings presented here exemplify how heterogeneity can have unexpected outcomes and the importance of examining heterogeneity for both natural and designed ECM constructs. Though traditional homogeneous environments will continue to provide knowledge, these substrates overlook the influence of ECM components on the spatial-temporal regulation of cell behavior. Though these preliminary results are still far from achieving decisively selective cell response, the methodology proposed here provides the first step toward mimicking the complexity of the ECM heterogeneity.

4. Conclusion

We introduced three facile methods for creating functionalized fibers and present the concept of combining these strategies to create an ordered, heterogeneous tissue scaffold. The use of such scaffolds reveals the synergistic influence of different peptides on the function of glia and neurite growth, revealing how such multimodal fabrication strategies might assist in both understanding the complexities of biological systems and providing tissue engineering solutions.

5. Experimental Section

Polymer Solutions Preparations: 300PEOT55PBT45, known commercially as PolyaActive 30055/45 (PA), a block copolymer of poly(ethylene oxide terephthalate) (PEOT), and poly(butylene terephthalate) (PBT), was provided by PolyVation B.V. (Groningen, The Netherlands). The chemical composition was represented by the notation $a\text{PEOT}b\text{PBT}c$, where a is the molecular weight, in g mol^{-1} , of the starting PEO segments, $(\text{C}_2\text{H}_4\text{O})_n$, used in the polymerization process, while b and c are the weight ratio between PEOT and PBT blocks, respectively. Based on the manufacturer's data $n = 7$ for the most abundant EO oligomer length was calculated. PA was used as main polymer, prepared as a 20% w/v solution dissolved overnight in a mixture of chloroform (CHCl_3) and 1,1,1,3,3,3-hexafluoro-2-propanol (HFIP) at a volume ratio of 7:3. The prefunctionalized agent was added 4 h before ESP under magnetic stirring at either a 5% or 2% w/v concentration. The three different prefunctionalization agents trialed in this study were PEG-bis(SVA), PEG-bis(Alkyne), and PEG-bis(Thiol) 5000 MW, provided by Laysan Bio (Alabama, USA). The same solutions were prepared for thin film formation time-of-flight secondary ion mass spectrometry (ToF-SIMS).

Electrospinning: Electrospinning was performed with a customized environmental chamber, maintained at a temperature of 25 °C and 30% humidity. The polymer solution was loaded into a syringe, mounted into a syringe pump and connected to a spinneret needle via Teflon

tubing to supply solution at a flow rate of 1 mL h^{-1} . The spinneret was mounted to a parallel plate, all of which was held at 20 kV and positioned 20 cm above the grounded collector. The collector was a gap electrode arrangement, with 2 mm wide electrodes and a 1 cm gap, producing aligned fibers across the gap. ESP fibers were collected onto mesh support rings made from a $450 \mu\text{m}$ thick polyester mesh (FinishMat 6691 LL (40 g m^{-2}), generously provided by Lantor B.V.), with a 15 mm outer diameter and 12 mm inner diameter, placed across the gap. ESP was performed for 1 min to achieve a sufficient fiber density. Heterogeneous scaffolds were produced via the Tandem ESP (T-ESP) technique.^[21] Briefly, heterogeneous scaffolds with two distinct, slightly overlapping populations of parallel fibers were deposited using the same electrode setup, substituting the single spinneret for two needles supplying different solutions mounted 1 cm apart. Divergent heterogeneous scaffolds were similarly generated by using a Y-shaped “epsilon” gap electrode to produce oriented fibers that overlap at a single location and diverge into two distinct fiber populations, greatly facilitating analysis of biological response.

ToF SIMS: Separate samples were prepared on $\approx 0.5 \text{ cm}^2$ segments of silicon wafer coated via evaporation of fluorooctyltrichlorosilane (FOTS, Sigma-Aldrich) in an enclosed chamber. Thin film control samples of polymer were prepared by spin coating (2000 rpm, 1 min) the polymer solution on to wafer segments. Silicon wafer segments were also prepared with ESP fibers by placing them between the gap of the target electrode. The same spinning parameters were employed as before.

ToF-SIMS was performed on a TOF.SIMS5 instrument (ION-TOF GmbH, Münster, Germany) at the Institute of Functional Interfaces, Karlsruhe Institute of Technology (KIT). The spectrometer was equipped with a Bi cluster primary ion source and a reflectron type time-of-flight analyzer. UHV base pressure was $< 5 \times 10^{-9}$ mbar. For high mass resolution the Bi source was operated in the “high current bunched” mode providing short Bi_1^+ or Bi_3^+ primary ion pulses at 25 keV energy and a lateral resolution of $\approx 4 \mu\text{m}$. The short pulse length of 1.1 to 1.3 ns allowed for high mass resolution. The primary ion beam was rastered across a $500 \times 500 \mu\text{m}^2$ field of view on the sample, and 128×128 data points were recorded. Primary ion doses were kept below 10^{11} ions cm^{-2} (static SIMS limit). If charge compensation was necessary an electron flood gun providing electrons of 21 eV was applied and the secondary ion reflectron tuned accordingly. Spectra were calibrated on the omnipresent C^- , C_2^- , C_3^- , or on the C^+ , CH^+ , CH_2^+ , and CH_3^+ peaks. Based on these datasets the chemical assignments for characteristic fragments were determined.

For high lateral resolution imaging the primary ion source was operated in nonbunched fast imaging mode. Here, only nominal mass resolution was obtained but the lateral resolution of the instrument was in the range of 150 nm. Therefore, peaks like S^- and HS^- were used for imaging since both peaks do not show other signals at the same nominal mass (m/z).

Fluorescent Label Conjugation: Reactivity and availability of functional groups were confirmed by the conjugation of fluorescent dyes with complementary binding motifs. SVA was conjugated to FITC-labeled BSA (Sigma) at $10 \mu\text{g mL}^{-1}$ in a PBS solution at pH 7.2. The thiol functional group was conjugated with a Dylight 488 maleimide probe (Invitrogen), which was applied at a concentration of $10 \mu\text{g mL}^{-1}$ in PBS. The click chemistry Alkyne functional group was conjugated with azido-labeled Megastokes 673 dye (Sigma) at a concentration of $10 \mu\text{g mL}^{-1}$ in PBS with $25 \times 10^{-3} \text{ M}$ ascorbic acid and $2.5 \times 10^{-3} \text{ M}$ copper (II) sulfate. Dye solutions were applied overnight. A T-ESP scaffold was simultaneously conjugated with a solution containing both the maleimide and azide probes (same concentrations). Substrates were washed three times with a tris buffered solution (TBS), pH 8, followed by a 1 h wash with a TRIS-based EDTA solution, pH 9, and then demineralized water (dH_2O) three times. To facilitate spatial analysis of observed neurite growth, T-ESP scaffolds conjugated the azide-Megastokes dye to the alkyne fibers as described above, but with a $50 \mu\text{g mL}^{-1}$ dye concentration incubated for 2 d.

Peptide Preparation: Both the click chemistry and the thiol strategies require functionalization of the biomolecule of interest with the

complementary binding partner. Peptide solutions of H-Gly-Arg-Gly-Asp-Ser-OH (RGD) and H-Arg-Asn-Ile-Ala-Glu-Ile-Ile-Lys-Asp-Ile-OH (RNIAEIIKDI; P20) (Bachem) were prepared at 5 mg mL^{-1} in PBS. These were activated with a maleimide and an azide, respectively, via amine-reactive linker molecules of NHS-peg4-Azide (Jena Bioscience) and sulfosuccinimidyl-4-(*N*-maleimidomethyl)cyclohexane-1-carboxylate (Sulfo-SMCC, Thermo Scientific). Maleimide and azide linker molecules were first dissolved in DMSO and then added to peptide solutions for a final linker concentration of 20 and $50 \times 10^{-3} \text{ M}$, respectively, representing a five times molar excess with respect to peptide concentration. Solutions were maintained at room temperature for 4 h. The SVA conjugating strategies did not require any pre-preparation of the proteins to be applied.

Scaffold Preparation: Glass cover slips (14 mm in diameter) were placed in a 24-well plate, followed by the ESP fibers collected on mesh rings; the glass cover slip provided a necessary mechanical support for subsequent removal and imaging of the electrospun mesh. A Viton rubber ring (Eriks B.V., The Netherlands) was inserted into the well to hold the scaffold in place. These constructs were placed inverted with respect to their fabrication orientation, such that the first deposited fibers were facing upward; the mesh ring provides a physical barrier between the ESP fibers and the Viton ring, improving handling during subsequent processing of cell culture samples. For homogeneously functionalized scaffolds, $150 \mu\text{L}$ of peptide solution was applied at a concentration of 0.5 mg mL^{-1} in PBS. Heterogeneous scaffolds were prepared using mixed peptide solutions at a concentration of 0.5 mg mL^{-1} of each peptide. Solutions involving click chemistry also had an additional $25 \times 10^{-3} \text{ M}$ of L-ascorbic acid and a $2.5 \times 10^{-3} \text{ M}$ Cu_2SO_4 (Sigma-Aldrich). Solutions were left over night to allow for conjugation. Similar to the fluorescent label conjugation, substrates were washed three times with a tris buffered solution (TBS), pH 8, followed by a 1 h wash with a TRIS-based ethylenediaminetetraacetic acid (EDTA) buffer (Klinipath B.V., The Netherlands), pH 9, and then dH_2O three times.

Cell Culture: Scaffolds were sterilized with 70% ethanol for 30 min, which was later left to evaporate. Scaffolds were washed three times with sterile PBS, followed by a one-time wash in Neuralbasal culture medium (Invitrogen) supplemented with B27 supplement, $0.5 \times 10^{-3} \text{ M}$ L-glutamine, 10 U mL^{-1} of penicillin/streptomycin (all from Invitrogen) and 10 ng mL^{-1} of NGF (Sigma-Aldrich). Culture plates were left to warm with $150 \mu\text{L}$ of culture medium per well in an incubator at $37 \text{ }^\circ\text{C}$ and 5% CO_2 . Dorsal root ganglia (DRGs) were extracted from 2 d old postnatal Sprague-Dawley rat pups. All procedures followed national and European laws and guidelines and were approved by the local ethical committee. Briefly, rats were sacrificed by cervical dislocation under general anesthesia (4% Isoflurane) and then decapitated. Individual ganglia were removed from the spinal column and nerve roots were stripped under aseptic conditions with the aid of a stereomicroscope. Connective tissue was removed and the DRGs were cut to expose the enclosed cells. One DRG was placed in the center of each ESP fiber scaffold; particular care was taken to ensure the DRG was placed in the overlapping region of the T-ESP scaffolds. Cultures were maintained for 5 d, with medium refreshed every other day.

Immunohistochemistry: Cells were first cooled to $4 \text{ }^\circ\text{C}$, followed by the addition of an equal volume of ice cold 4% w/v paraformaldehyde (PFA) in PBS, added to each well for a final concentration of 2% PFA. Fixation proceeded for 20 min, after which samples were washed with TBS. Samples were permeabilized with 0.1% Triton-X for 15 min, washed two times with TBS and blocked with 5% normal goat serum for 1 h. This was followed by a 16 h incubation at $4 \text{ }^\circ\text{C}$ in a 1:1000 dilution of BIII-tubulin (Sigma) raised in mouse, and 1:500 S100 (Sigma) raised in rabbit in TBS with 1% normal goat serum. Samples were then washed three times in TBS with 1% normal goat serum, secondary antibody of antimouse Alexa 488 or Alexa 546 raised in goat (Invitrogen) and antirabbit Atto 647N raised in goat (Sigma) were applied at a dilution 1:500 for 12 h at $4 \text{ }^\circ\text{C}$. Samples were then washed three times with TBS containing 1% BSA and 0.1% w/v sodium azide (Sigma-Aldrich). After staining, the alkyne-containing fibers of the T-ESP scaffolds were selectively labeled as outlined in the *Fluorescent Label conjugation* section

above. Samples were washed again with TBS, then removed from the well and mounted on a coverslip using 4–88 mowiol mounting fluid with 2.5% w/v 1,4-diazabicyclo[2.2.2]octane (DABCO, Sigma-Aldrich) for microscopy imaging.

Microscopy and Image Analysis: Fluorophore conjugation to fibers was imaged using a Nikon TI confocal microscope, eliminating diffractive autofluorescence. Per fluorophore, laser power was adjusted using the conjugated scaffolds as a reference. The remaining scaffolds were imaged using the same power settings to determine the degree of selective conjugation. Cell labels were imaged using a BD Pathway 435 with a 4× objective. Neurites were imaged via the Alexa 488 or Alexa 546 labels, using the ex: 482/35-em: 536/40 or ex: 543/22-em: 593/40 filter sets, respectively (ex: excitation; em: emission). Schwann cells were visualized with the Atto 647N fluorophore using an ex: 628/40-em: 692/40 filter set. The use of Megastoke 678 dye made possible the visualization of alkyne fibers by using an ex: 543/22-em: 692/40 filter set. To facilitate comparison of neurite length between samples with diverging and nonlinear neurite growth, a custom ImageJ script was developed to automatically determine the net direction of growth and map pixel intensities to Cartesian coordinates centered around this growth direction (detailed in Figure S1, Supporting Information). The same approach was used to assess both neurite extension and Schwann cell migration. Images shown were processed using the Contrast Limited Adaptive Histogram Equalization (CLAHE) filter within the ImageJ/Fiji software package, with stitched mosaic created with the Grid Stitch plug-in.^[31]

Statistical Analysis: All statistics were performed with R statistical software (<http://www.R-project.org/>). Comparisons of fiber diameters and fiber alignments were performed with a one way ANOVA followed by a posthoc Holm method, with significance level of $p < 0.01$ and a minimum of 100 fibers measured per fiber type. To determine the average neurite extension and Schwann cell migration, the mean per sample was first calculated of the farthest 15 measurable points and these values were then averaged. A nonparametric Mann-Whitney-Wilcoxon unpaired test was used to determine significance between the P20 and RGD conditions.

Supporting Information

Supporting Information is available from the Wiley Online Library or from the author.

Conflict of Interest

The authors declare no conflict of interest.

Keywords

divergent patterns, electrospinning, functionalization, neural tissue, peptides

Received: March 24, 2020

Revised: June 27, 2020

Published online:

- [1] M. W. Tibbitt, K. S. Anseth, *Biotechnol. Bioeng.* **2009**, *103*, 655.
- [2] R. G. Wylie, S. Ahsan, Y. Aizawa, K. L. Maxwell, C. M. Morshead, M. S. Shoichet, *Nat. Mater.* **2011**, *10*, 799.
- [3] J. S. Miller, K. R. Stevens, M. T. Yang, B. M. Baker, D.-H. T. Nguyen, D. M. Cohen, E. Toro, A. A. Chen, P. A. Galie, X. Yu, R. Chaturvedi, S. N. Bhatia, C. S. Chen, *Nat Mater.* **2012**, *11*, 768.
- [4] S. K. Seidlits, C. E. Schmidt, J. B. Shear, *Adv. Funct. Mater.* **2009**, *19*, 3543.
- [5] Q. P. Pham, U. Sharma, A. G. Mikos, *Tissue Eng.* **2006**, *12*, 1197.
- [6] H. Cao, T. Liu, S. Y. Chew, *Adv. Drug Delivery Rev.* **2009**, *61*, 1055.
- [7] M. Jassal, S. Sengupta, S. B. Warner, S. Bhowmick, *Text. Res J.* **2013**, *83*, 1999.
- [8] B. Carlberg, T. Wang, J. Liu, *Langmuir* **2010**, *26*, 2235.
- [9] K.-N. Chua, W.-S. Lim, P. Zhang, H. Lu, J. Wen, S. Ramakrishna, K. W. Leong, H.-Q. Mao, *Biomaterials* **2005**, *26*, 2537.
- [10] H. G. Sundararaghavan, R. B. Metter, J. A. Burdick, *Macromol. Biosci.* **2010**, *10*, 265.
- [11] R. Delgado-Rivera, J. Griffin, C. L. Ricupero, M. Grumet, S. Meiners, K. E. Uhrich, *Colloids Surf., B* **2011**, *84*, 591.
- [12] P. Liesi, A. Narvlnen, H. Sariola, G. Snounou, *FEBS Lett.* **1989**, *244*, 141.
- [13] S. Lindström, H. Andersson-Svahn, *Lab Chip* **2010**, *10*, 3363.
- [14] M. Théry, *J. Cell Sci.* **2010**, *123*, 4201.
- [15] R. G. Wylie, M. S. Shoichet, *J. Mater. Chem.* **2008**, *18*, 2716.
- [16] C. a. DeForest, B. D. Polizzotti, K. S. Anseth, *Nat. Mater.* **2009**, *8*, 659.
- [17] T. G. Kim, T. Park, D. Ph, *Tissue Eng.* **2006**, *12*, 221.
- [18] A. Lancuški, S. Fort, F. Bossard, *ACS Appl. Mater. Interfaces* **2012**, *4*, 6499.
- [19] F. Lin, J. Yu, W. Tang, J. Zheng, S. Xie, M. L. Becker, *Macromolecules* **2013**, *46*, 9515.
- [20] D. Grafahrend, K.-H. Heffels, M. V. Beer, P. Gasteier, M. Möller, G. Boehm, P. D. Dalton, J. Groll, *Nat. Mater.* **2011**, *10*, 67.
- [21] P. Wieringa, R. Truckenmuller, S. Micera, R. Van Wezel, L. Moroni, *Biofabrication* **2020**, *12*, 025010.
- [22] H. Fong, I. Chun, D. H. Reneker, *Polymer* **1999**, *40*, 4585.
- [23] M. Barczyk, S. Carracedo, D. Gullberg, *Cell Tissue Res.* **2010**, *339*, 269.
- [24] W.-Q. Liu, J. A. Martinez, J. Durand, W. Wildering, D. W. Zochodne, *Neurobiol. Dis.* **2009**, *34*, 11.
- [25] T. G. Santos, F. H. Beraldo, G. N. M. Hajj, M. H. Lopes, M. Roffe, F. C. S. Lupinacci, V. G. Ostapchenko, V. F. Prado, M. A. M. Prado, V. R. Martins, *J. Neurochem.* **2013**, *124*, 210.
- [26] C. Webber, D. Zochodne, *Exp. Neurol.* **2010**, *223*, 51.
- [27] E. Masaeli, P. A. Wieringa, M. Morshed, M. H. Nasr-Esfahani, S. Sadri, C. A. Van Blitterswijk, L. Moroni, *Nanomedicine* **2014**, *10*, 1559.
- [28] P. C. Kerstein, R. H. NicholIV, T. M. Gomez, *Front. Cell. Neurosci.* **2015**, *9*, 244.
- [29] J. P. Myers, T. M. Gomez, *J. Neurosci.* **2011**, *31*, 13585.
- [30] E. P. Mccurdy, K. M. Chung, C. R. Benitez-agosto, U. Hengst, *Cell Rep.* **2019**, *29*, 363.
- [31] S. Preibisch, S. Saalfeld, P. Tomancak, *Bioinformatics* **2009**, *25*, 1463.